Ring Diagram Analysis with GONG++

T. Corbard, C. Toner, F. Hill, K. D. Hanna

GONG/NSO, Tucson, Arizona

D. Haber, B. Hindman

JILA, Boulder, Colorado

R. Bogart

CSSA, HEPL, Stanford Univ, California

Motivations

Images from the updated GONG network (GONG+) have been produced since July 2001. In order to treat individual site images and the merged images (See the poster from Toner et al.) for local helioseismology studies, we have developed an enhanced tracking/remapping code that is now part of the new GONG pipeline (GONG++) (see the poster from Hill et al.).

We present here some features of the tracking code and compare the preliminary results using GONG+ images with the ring diagram analysis of MDI images for the same days.

The principal objectives of this work are to detect the solar sub−surface flows in both azimuthal and meridional directions and in both solar hemispheres and to study the behavior of these flows around magnetic features and during the solar cycle with both GONG+ and MDI data.

The tracking/remapping code

The choice of the grid

The area to be tracked can be defined on a reference image either on a Latitude−Longitude grid or on a grid of points along great circles. The difference between the two choices become important only at high latitudes. The Great Circle grid correspond to an azimuthal equidistant (or Postel) projection and is more appropriate for local analysis where the high degree acoustic waves are assimilated to plane waves traveling across the surface of the Sun following geodesics (Haber et al. 1995).

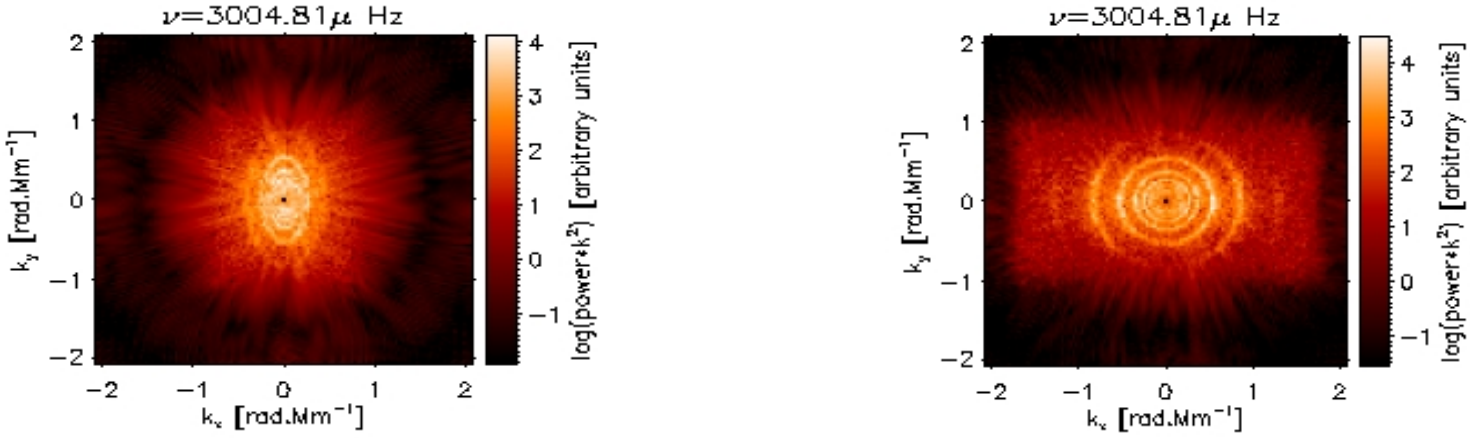

Rings obtained by tracking a 16° x 16° region centered at 65° of latitude 0° of longitude (at the middle of the run) for 1664mn.

At this high latitude, rings are clearly identified only when using the great−circle (or Postel) projection (right) and strongly distorted when using a Latitude−Longitude grid (left).

The choice of the tracking rate.

Apart from the case where we choose not to track a region but to look at a constant location on our solar images, we have to take into account the rotation rate of the surface of the Sun. There are 3 basic choices:

1)The Carrington rate (~13.2 deg/day).

−>It allows the tracked area to be always identified by the Carrington coordinates of its center but

−>it assumes a rigid rotation rate and does not take into account the known differential rotation rate in latitude.

2)**All pixels of the area are tracked at the rate of the center of the area.**

−>The area can be defined by the Carrington coordinates of its center only on the reference image.

−>If the latitudinal extent of the area is important, the tracking rate may not be appropriate for the most extreme latitudes.

3)**Each latitude is tracked independently: shearing coordinate system**

−>The tracking rate is appropriate for all pixels but

−>If the grid is chosen along Great Circles, this will be true only on the reference image.

The standard choice is 2)

The choice of the interpolator

In order to go from camera pixels to the chosen grid (Latitude − Longitude or Great Circles), we need to do some interpolation. Two choices are allowed:

1) The 'ideal sinc interpolator' defined (in 1D) by:

$$f(x)=\sum_{n=-N}^{n=N-1} \frac{\pi(x-n)}{2N\tan\left(\frac{\pi(x-n)}{2N}\right)} \quad \sin\frac{(\pi(x-n))}{\pi(x-n)} \quad f(n)$$

This can be seen as a tapered version of the sinc interpolator where the taper is 'ideal' for the Discrete Fourier Transform in the sense that if we were to shift the image by an arbitrary fraction of pixels using this interpolator the DFT would remain the same except for a phase.

−>A similar interpolator (slightly different tapering function) is used during the merging of individual site images. It is probably good to keep the same interpolator in both steps.
−>Good frequency response if we take enough points (N=15) but
−>Time consuming
−>Since we are interpolating the image at arbitrarily distributed points, we are not only shifting but also stretching the image. Therefore it is not obvious that this interpolator is ideal for us.

2) The spline interpolator based on a tensorial product of B−splines. (De Boor, 1978)

−>Good frequency response even for low order (cubic) piecewise polynomials
−>The spline computation is based on finite differences which are very easy and fast to implement numerically (5 time faster than the sinc interpolator)

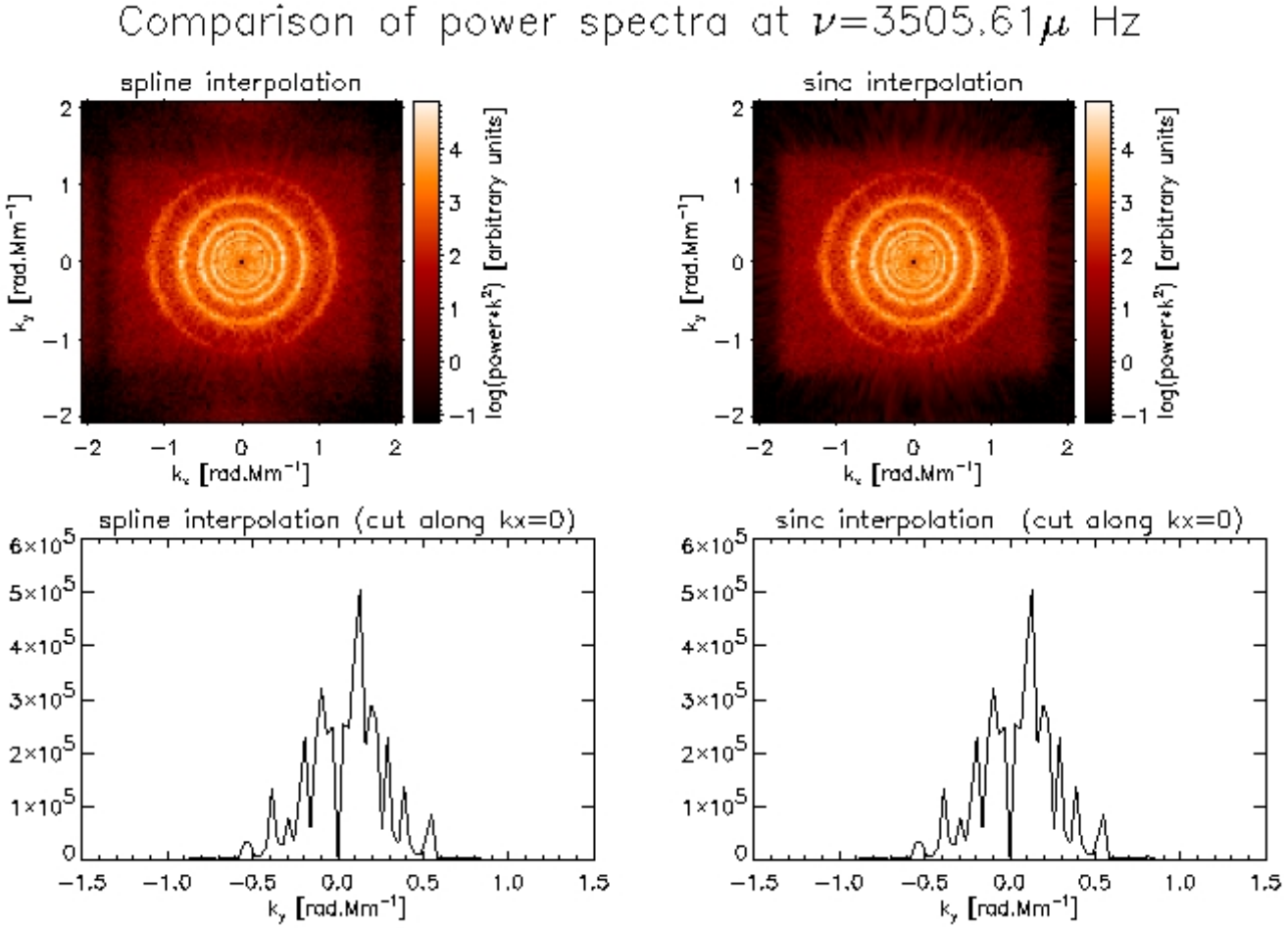

The power spectra obtained using the spline or sinc interpolator are very similar.
In the upper images the logarithm of the power times k^2 is shown in order to enhance the visibility of outer rings. The two lower plots show cuts of the power spectra themselves (no enhancement factor and no logarithm taken) along $k_X=0$.

No difference between the two spectra can be seen on these plots execpt for the noise at very high spatial frequencies that seems higher when using the spline interpolator.

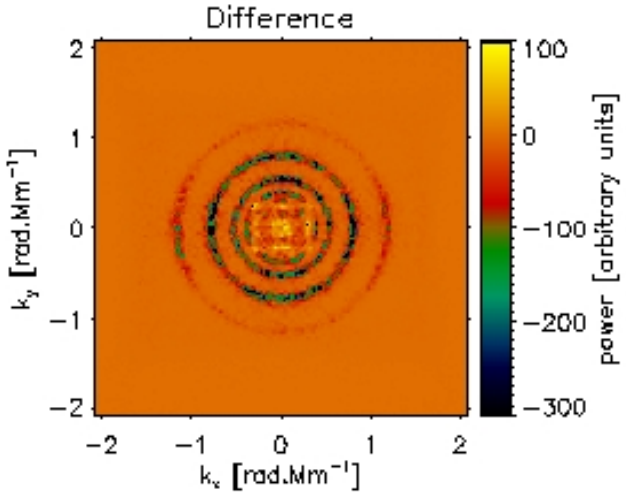

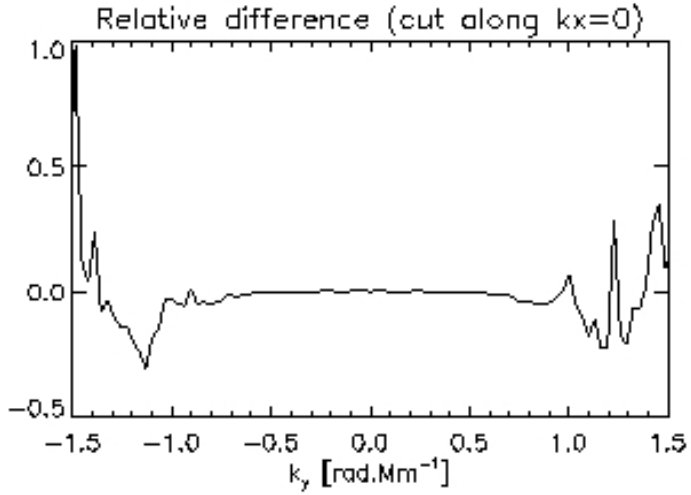

By plotting the difference of the power spectra obtained from spline and sinc interpolator we realize that a difference exists which is principally concentrated on the rings. This difference is however very small and the relative difference is essentially zero for $|k_X|<1$ Mm/s.

Therefore it seems that only the very outer ring could potentially be affected by the choice of the interpolation.

The real test however to know if we can use the faster spline interpolator will be to check if it leads to any difference on the final result i.e. the flow maps. This comparison is under way.

From the maps to the 3D Power spectra

The data cube of a tracked area is fourier transformed via a 3D FFT.
This requires first a spatial and a temporal apodization in order to avoid truncation effects.

Spatial apodization

We have chosen a 2D cosine bell apodization in the spatial direction reducing a 16° x 16° area to a circular patch of radius 15° .

Multitaper Analysis

The temporal apodization is done using a muiltitaper technique. This method has been sucessfully used in global helioseismology (Kras et al.). It consists in aplying a sequence of tapers, taken orthogonal over the window function, before doing the temporal FFT and then to average the resulting power spectra.
Doing so we avoid the lost of data that would result from the use of a single taper and we reduce the effect of the leakage induced by the window function (Percival & Walden 1993). The result is a much smoother power spectrum resulting from a better distribution of the power along the rings.
Applying too many tapers would result in an over−smoothed power spectrum and therefore a trade−off has to be found. We are still performing tests to validate the use of multitaper analysis in local helioseismology.

Effect of a temporal multitaper analysis on the power spectra

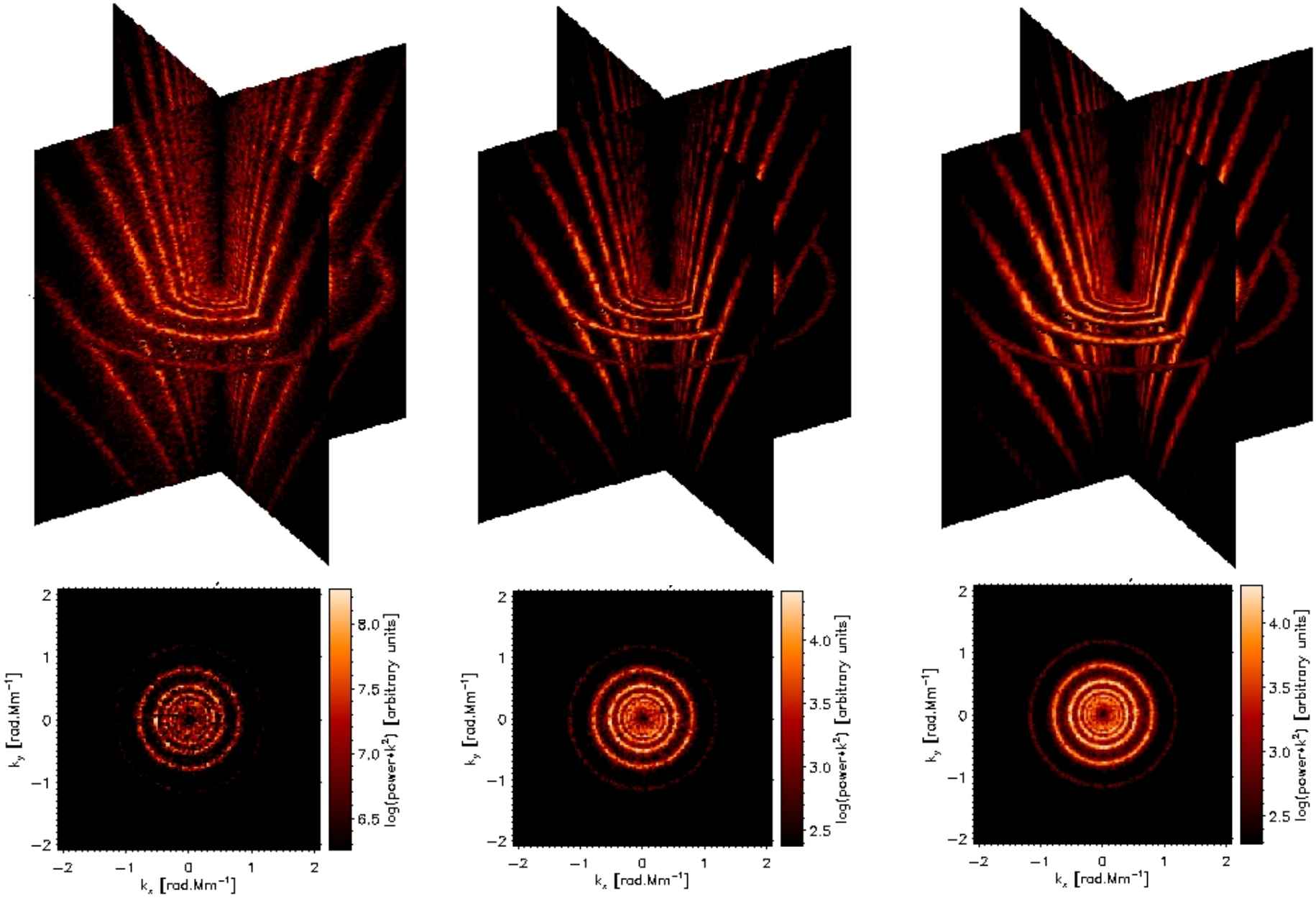

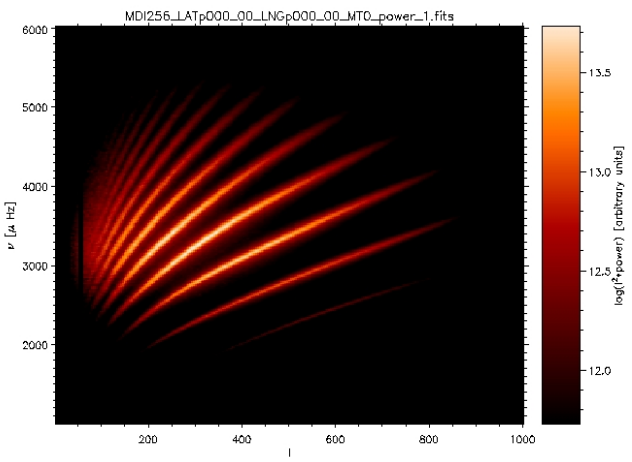

No taper

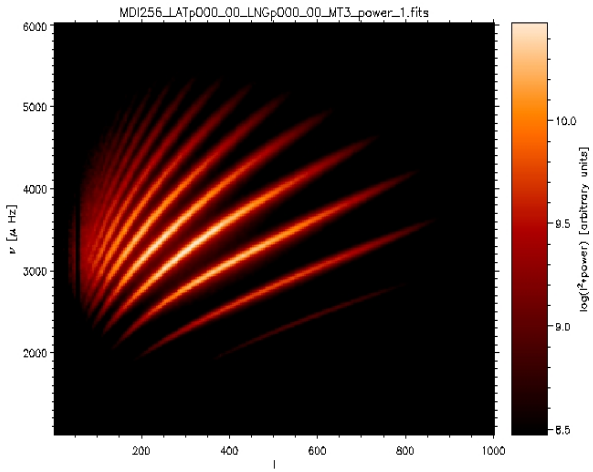

3 Tapers

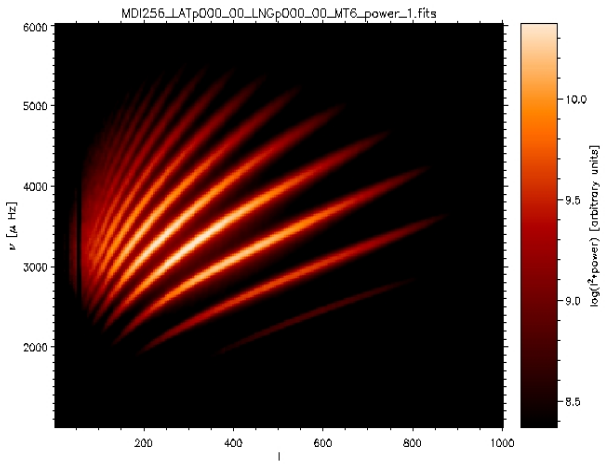

6 Tapers

These figures illustrate the smoothing effect of the multitaper analysis.

First row : 3D power spectra
Second row: Cut at ν=3500μHz
Third row : Average power spectra (l−ν diagrams)

The first tests show that multitapering helps the fitting of the power spectra.

First results: the flow maps at different depths from a dense−pack analysis of GONG+ merged images

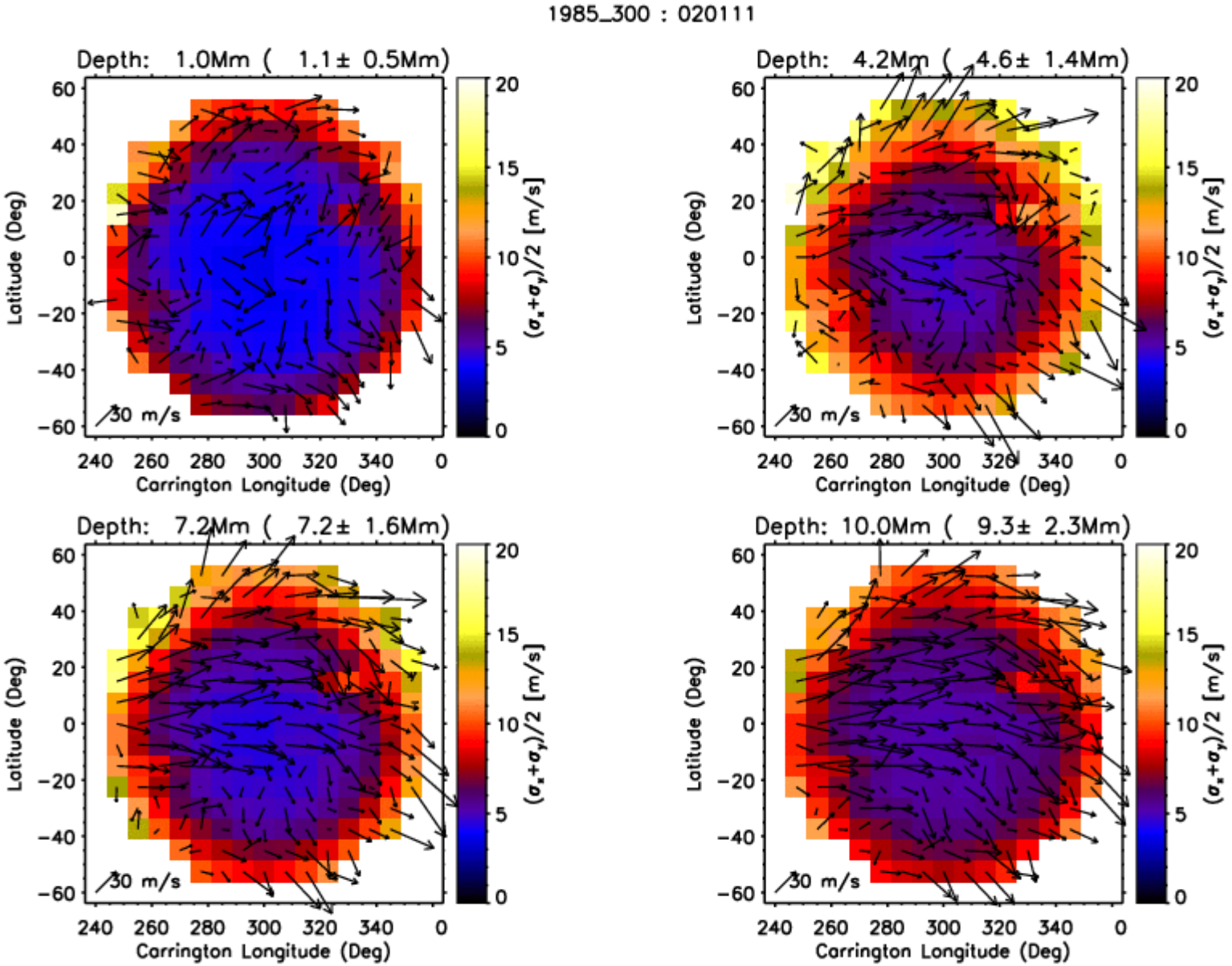

Existing codes, previously used on MDI data, have been adapted to analyse a dense−pack of tracked areas (Haber et. al., 2000): 189 areas of 16°x16° distributed between 52.5° of latitude and 52.5° of longitude and tracked on the GONG+ merged images during 1664 minutes).
The 3D power spectra of different tracked areas, which present the characteristic rings distorted by the underlying flows, are fitted using a Maximum Likelihood method to extract the EW and NS components of the flow.These components are finally inverted using a Regularized Least Square method in order to obtain the depth dependence of the flow down to 15Mm below the photoshere.
All the computations where made using the new GONG++ pipeline that is currently being developped using the Operations Pipeline Unified System (OPUS).
The results at 4 different depths for January 11 2002 are shown above. The background color levels represent the averaged errors of the x and y components of the velocity vector.
This figures show that the lowest errors are reached at a depth of about 1−1.5Mm. We have therefore chosen this depth for the first comparison between GONG and MDI ring diagram analysis.

GONG++ / MDI ring diagram analysis comparison

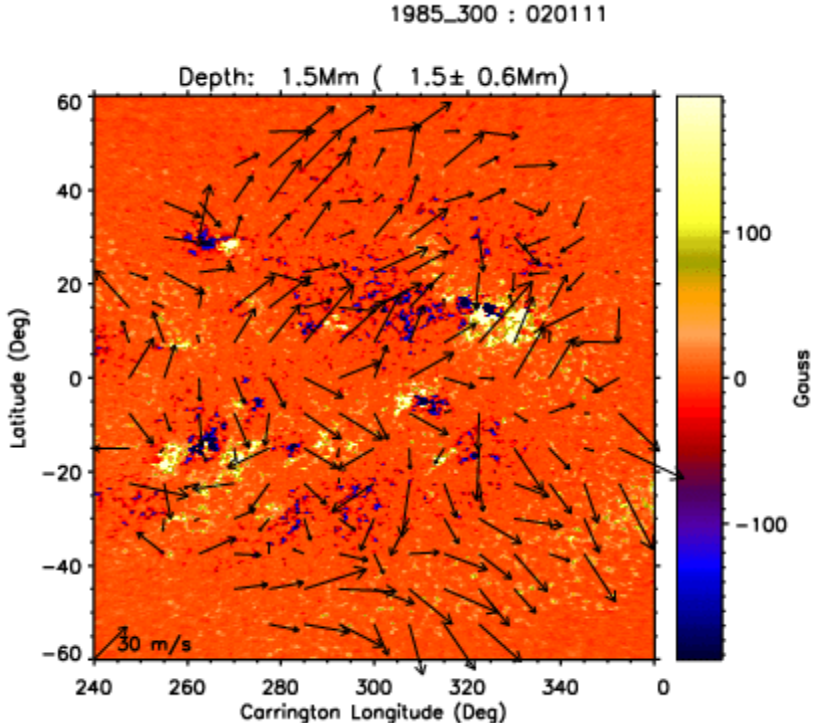
1985_300 : 020111
Depth: 1.5Mm (1.5± 0.6Mm)
Latitude (Deg)
Carrington Longitude (Deg)
Gauss
30 m/s

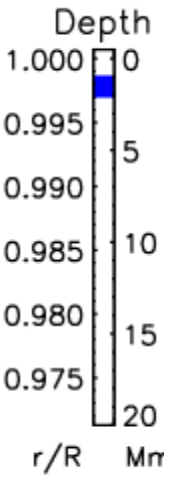
Depth
1.000
0.995
0.990
0.985
0.980
0.975
0
5
10
15
20
r/R
Mm

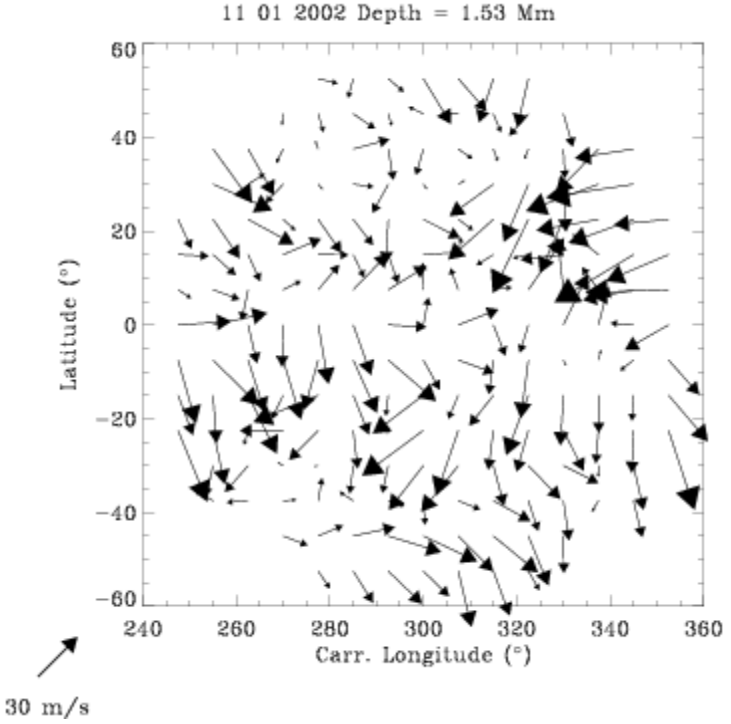
11 01 2002 Depth = 1.53 Mm
Latitude (°)
Carr. Longitude (°)
30 m/s

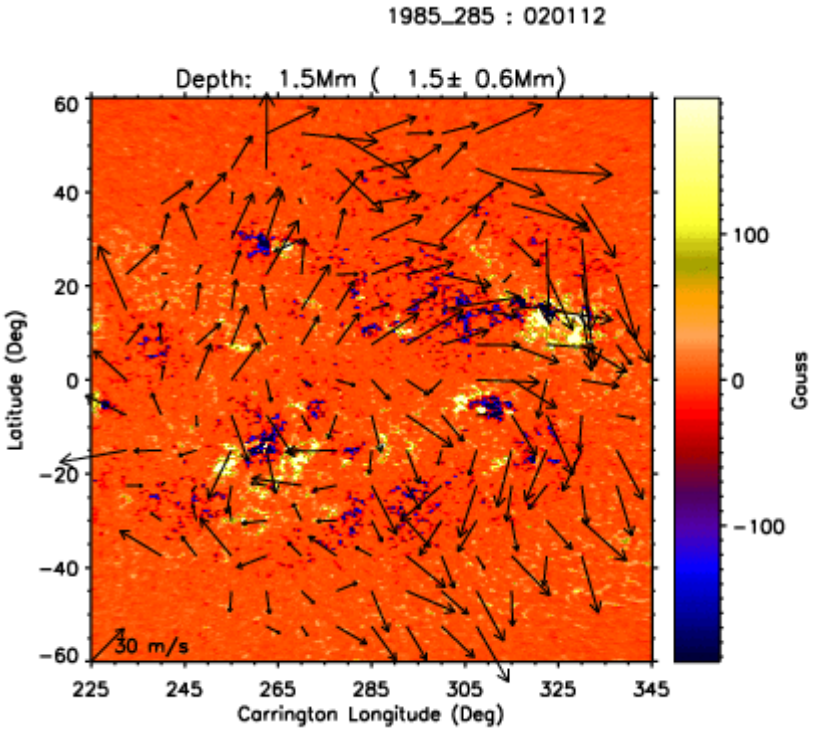
1985_285 : 020112
Depth: 1.5Mm (1.5± 0.6Mm)
Latitude (Deg)
Carrington Longitude (Deg)
Gauss
30 m/s

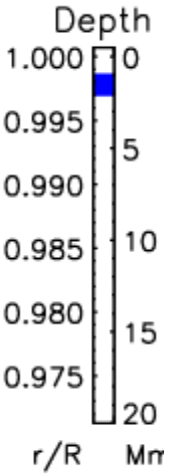
Depth
1.000
0.995
0.990
0.985
0.980
0.975
0
5
10
15
20
r/R
Mm

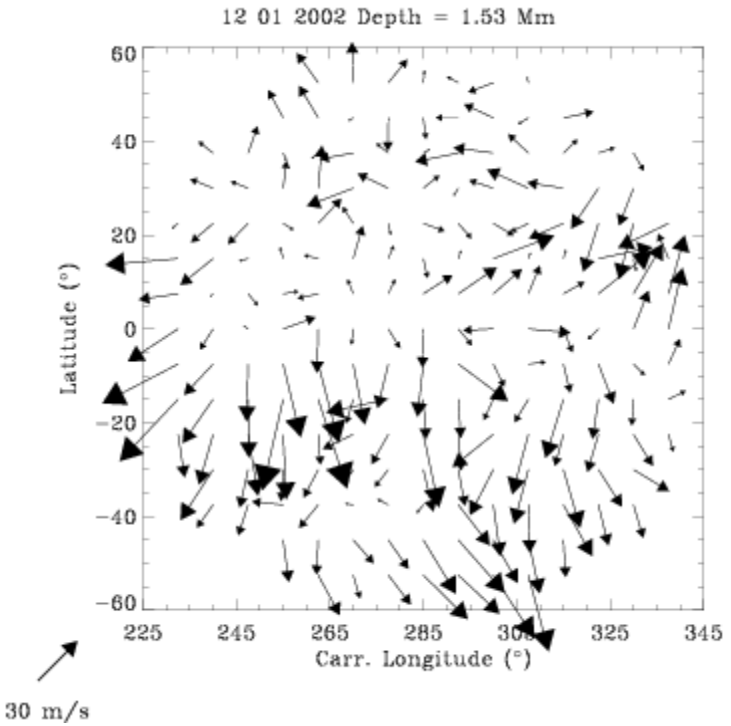
12 01 2002 Depth = 1.53 Mm
Latitude (°)
Carr. Longitude (°)
30 m/s

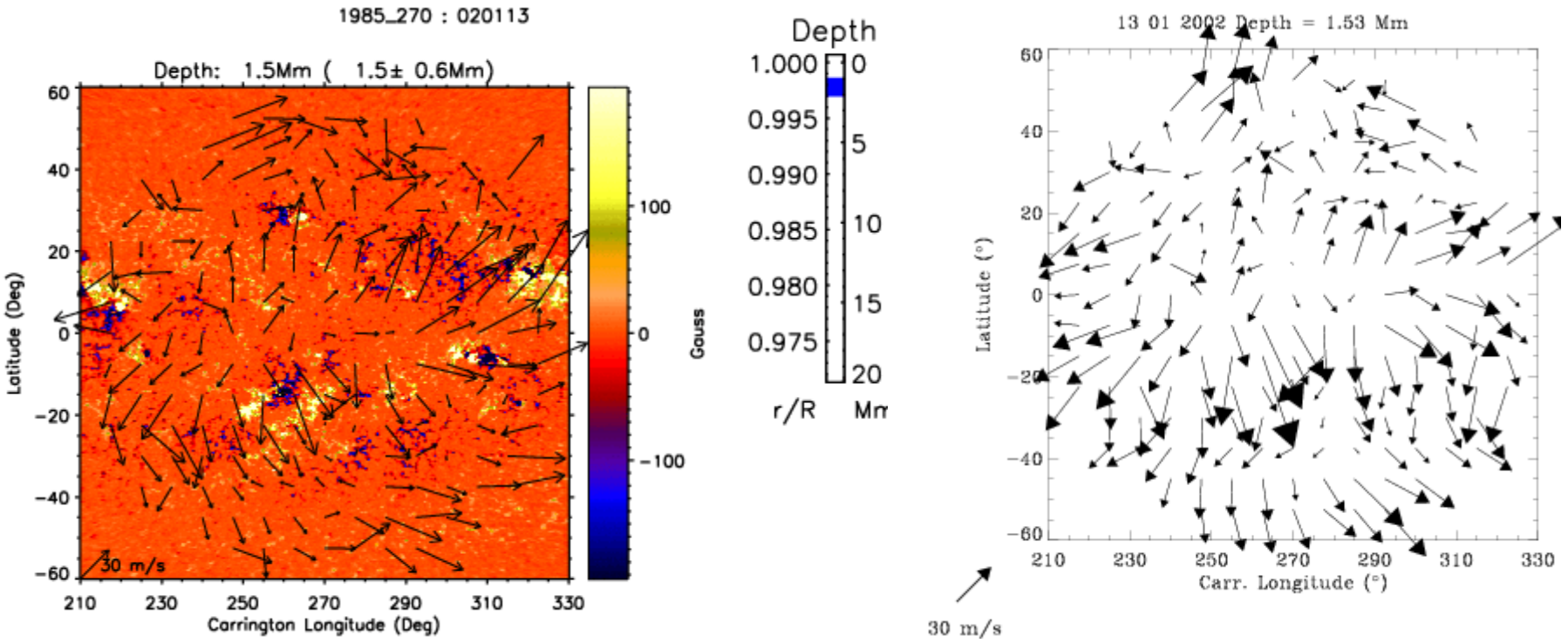

These maps compare the flows obtained separately from GONG (left) and MDI (right) velocity images for three different and consecutive days (January 11−12−13 2002 from top to bottom). The GONG results are presented with the GONG+ magnetograms for that day as background and an estimate of the radial resolution achieved at that depth (1.5Mm).

The two results seems to be in reasonably good qualitative agreement but present also some important differences that need to be investigated further. An intensive and quantitative comparison of the two data sets and analysis techniques is being started with this first results.

The hope is that this comparison will soon allow us to become more confident about the reliability of the inferences made about the meridional circulation and the dynamic around active regions previously made only from MDI data.

References:

De Boor, C., 1978, A practical Guide to Splines, Springer Verlag.

Haber, D. A., Hill, F., Gough D., 1995, GONG'94, ASP Conf Series 76, p. 272

Haber, D. A., Hindman, B. W., Toomre, J., Bogart, R. S., Thompson, M. J., Hill, F., 2000, Solar Physics 192, 335

Hill, F., Bolding J., Toner C., Corbard T., Wampler S., Goodrich B., Goodrich P., Eliason P., 2002, The GONG ++ data processing pipeline, poster, this meeting

Kras, S., Howe, R., Komm, R., Hill, F., 2002, New result from GONG 'classic' data, SPD 2002

Percival D. B & Walden A. T., 1993, Spectral Analysis for Physical Applications, Cambridge University Press.

Toner, C., Haber, D. A., Bogart, R. S., Hindman, B. W., 2002, An Image merge for GONG+, poster, this meeting